A Study on the Rotating Ring Using Air Bearing in Yarn Manufacturing Process

Seung-Ho Jang*

(논문접수일 2010. 2. 9, 심사완료일 2010. 7. 5)

방적공정에 있어서 공기 베어링을 이용한 회전링에 관한 연구

장승호*

Abstract

The increase of the spindle speed to enhance the productivity in ring spinning processes has been limited by yarn tension and heat generation of the traveller/ring. The main causes of yarn tension are 1) the force added directly to the yarn by the rotation of the spindle and 2) the centrifugal force exerted by the yarn balloon generated by traveller rotation. The dominant causes of heat generation are 1) the friction between the ring and traveller and 2) the friction between the traveller and yarn. These factors cause yarn end-breaks and heat damage. In the case of the staple yarn manufacturing process for PET (polyester) and nylon (a heat plasticity material), the rotational speed of the ring spinning system has deteriorated to 10,000rpm. The objective of this study was to develop a rotating ring which has dynamic stability, high productivity and a simple structure to overcome the limitations of the conventional fixed ring/traveller system. The results of this study revealed that the spinning tension could be reduced by 67.8% using the newly developed rotating ring.

Key Words : Rotating Ring(회전링), Air Bearing(공기 베어링), Spinning Process(스피닝 공정), Dynamic Stability(동적 안정성), Moment of inertia(관성 모멘트)

1. Introduction

The spinning process in yarn manufacturing has a more direct effect on the quality and productivity of textile products than any other unit process. Until now, seven kinds of spinning processes have been developed, and include 1) the ring spinning process, 2) the open end spinning process, 3) the cap spinning process, 4) the mule spinning process, 5) the self twist spinning process, 6) the air jet spinning process, and 7) the flyer spinning process[1].

These processes produce yarns with different properties. Among these processes, the ring spinning process is the standard to which products produced by the other processes are compared, since this process produces products of the best quality.

The ring spinning system consists of five parts: the feeding part, the drafting part, the twisting part, the winding part and the copping part[2]. The mechanism of this system is to twist the sliver and continuously transform the yarn thickness through the rotation of the traveller, which moves in a circular orbit. The yarn is wound sequentially in the bobbin which is fixed in the spindle(refer to Fig. 1). The efficiency of this ring spinning
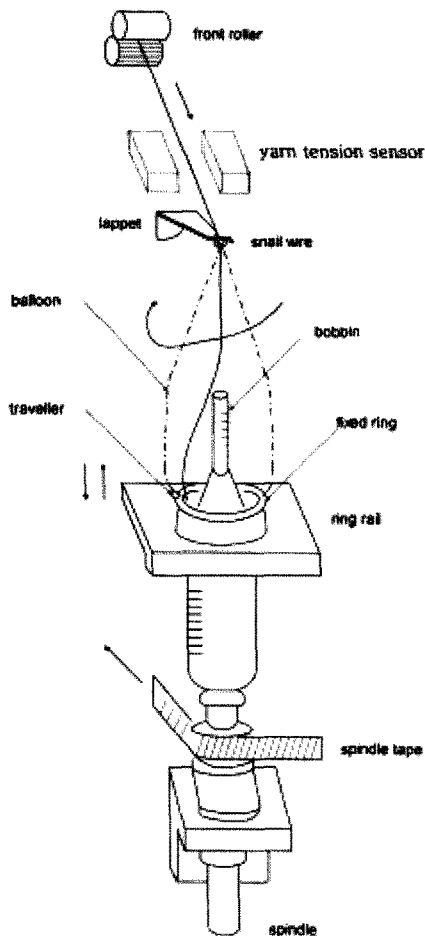
system is limited by the yarn tension and the heat generation of the traveller/ring. The main causes of increases in yarn tension are the forces added directly to the yarn by the rotation of the spindle and the centrifugal forces of the yarn balloon, which is generated by the rotation of the traveller[3].

The dominant causes of heat generation are the friction between the ring and the traveller and the friction between the traveller and the yarn. These factors cause end-breaks and heat damage of the yarn. In the case of the staple yarn manufacturing process for the PET(polyester) and nylon(heat plasticity material), the rotational speed of the ring spinning system deteriorated to 10,000rpm.

The objective of this study was to develop a rotating ring which has dynamic stability, high productivity and a simple structure to overcome the limitations of the conventional fixed ring/traveller system.

2. Equation of motion of a rotating ring

The rotating ring is set on a fixed coordinate system (X, Y and Z) and rotational coordinate system (X', Y' and Z') in order to mathematically describe its motion, as shown in Fig. 2. In general, a rigid body which is moving in three dimensional space has six degrees of freedom and is subject to both rotational and translational motions. Equations of these motions can be described by the following differential equations[3].
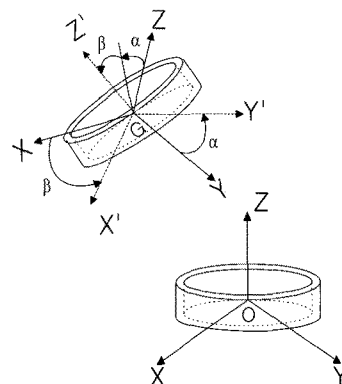

Fig. 1 Ring spinning system

Fig. 2 Coordinate systems of a rotating ring

$$\frac{d^2x}{dt^2} = -\frac{a}{m_r}x + \frac{m_r r_t^2 r_1 \cos\theta}{m_r} \tag{1}$$

$$\frac{d^2y}{dt^2} = -\frac{a}{m_r}y + \frac{m_r r_t^2 r_1 \cos\theta}{m_r} \tag{2}$$

$$\frac{d^2z}{dt^2} = -\frac{b}{m_r}z - g \tag{3}$$

$$\frac{d^2\alpha}{dt^2} = -\frac{I_z}{I_X}r_0\frac{d\beta}{dt} + \frac{fr_1\sin\theta}{I_X} \tag{4}$$

$$\frac{d^2\beta}{dt^2} = \frac{I_z}{I_X}r_0\frac{d\alpha}{dt} - \frac{fr_1\cos\theta}{I_X} \tag{5}$$

$$\frac{d^2\gamma}{dt^2} = -\frac{\eta}{I_z}\frac{d\gamma}{dt} + \frac{\mu fr_1 - \tau_s\sin\theta}{I_z} \tag{6}$$

Equations (1), (2) and (3) describe the translational motion of the rotating ring in the yarn spinning process. Equations (4), (5) and (6) describe the rotational motion of the rotating ring. From these equations, Jang, et al[3-6]. verified that the shape of the rotating ring using an air bearing should satisfy the inequality $I_x/I_z > 1.0$ for stable rotation in the spinning process(here, I_x/I_z is called the moment of inertia ratio(MIR)).

3. Design of a rotating ring

3.1 Moment of inertia ratio (MIR) for rotating rings

In this research, the author devised and named forty-four kinds of air bearings for the rotating ring.

The rotating ring of a one-stage rectangular type listed in Fig. 3(1) is shown in Fig. 4. This rotating ring consists of three parts(l_1, l_2, l_3) and the mass of each part is determined from Equations (7), (8) and (9) respectively,
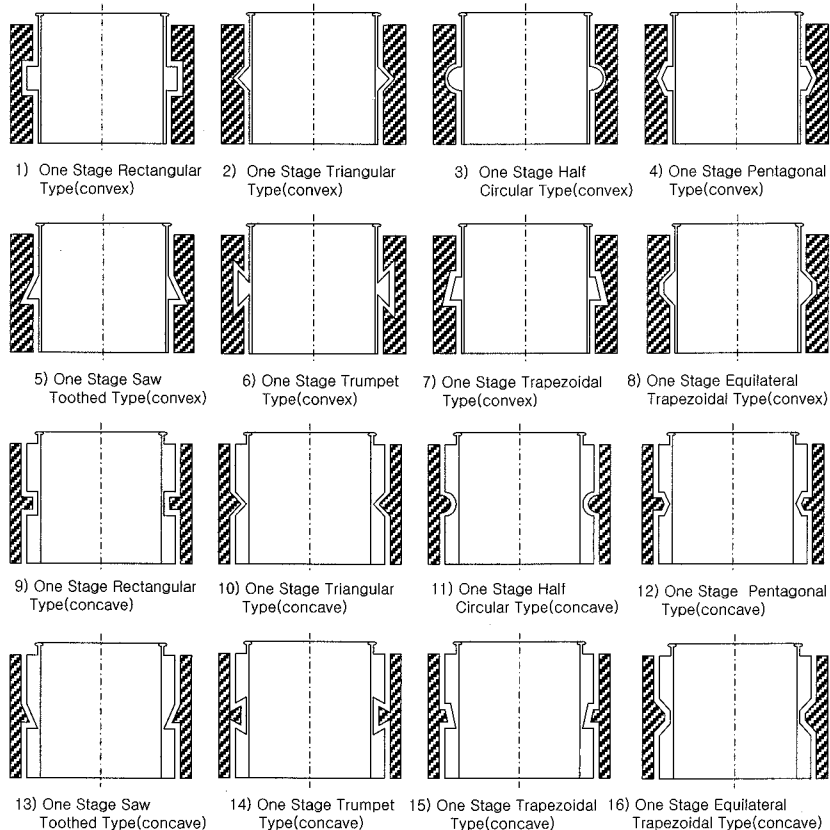

1) One Stage Rectangular Type(convex)   2) One Stage Triangular Type(convex)   3) One Stage Half Circular Type(convex)   4) One Stage Pentagonal Type(convex)

5) One Stage Saw Toothed Type(convex)   6) One Stage Trumpet Type(convex)   7) One Stage Trapezoidal Type(convex)   8) One Stage Equilateral Trapezoidal Type(convex)

9) One Stage Rectangular Type(concave)   10) One Stage Triangular Type(concave)   11) One Stage Half Circular Type(concave)   12) One Stage Pentagonal Type(concave)

13) One Stage Saw Toothed Type(concave)   14) One Stage Trumpet Type(concave)   15) One Stage Trapezoidal Type(concave)   16) One Stage Equilateral Trapezoidal Type(concave)

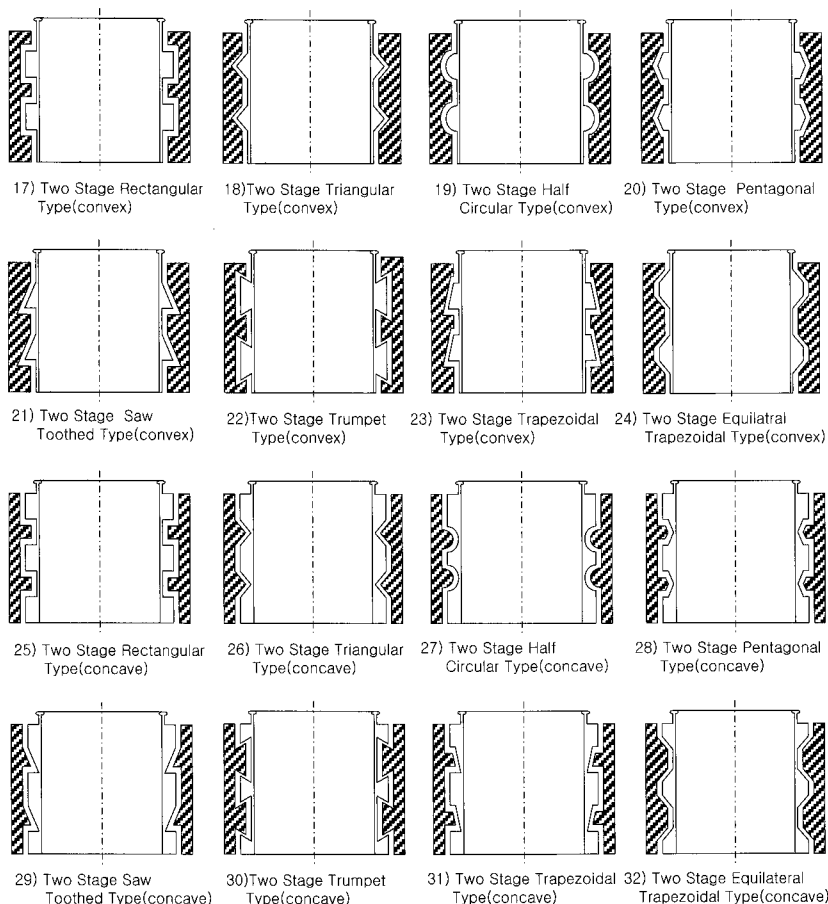**Fig. 3 Rotating ring shape (1)**

Fig. 3 Rotating ring shape (2)

where, r_1 is the inner radius of the rotating ring, r_2 is the outer radius of the rotating ring and r_3 is the distance from the center of the rotating ring to the edge of the rotating ring.

$$m_1 = \rho\pi(r_2^2 - r_1^2)l_1 \tag{7}$$

$$m_2 = \rho\pi(r_3^2 - r_1^2)l_2 \tag{8}$$

$$m_3 = \rho\pi(r_2^2 - r_1^2)l_3 \tag{9}$$

The center of gravity can be described as follows:

$$\bar{z} = \frac{l_1(l_3 + l_2 + l_1/2)(r_2^2 - r_1^2) + l_2(l_3 + l_2/2)(r_3^2 - r_1^2) + l_3(l_3/2)(r_2^2 - r_1^2)}{l_1(r_2^2 - r_1^2) + l_2(r_3^2 - r_1^2) + l_3(r_2^2 - r_1^2)} \tag{10}$$

The moment of inertia on the X axis for each part of the rotating ring(l_1, l_2, l_3) can be obtained by the following equations, respectively:

$$I_{X1} = m_1\left[\frac{1}{12}l_1^2 + \frac{1}{4}(r_2^2 + r_1^2) + (l_3 + l_2 + l_1/2 - \bar{z})^2\right] \tag{11}$$

$$I_{X2} = m_2\left[\frac{1}{12}l_2^2 + \frac{1}{4}(r_3^2 + r_1^2) + (l_2 + l_1/2 - \bar{z})^2\right] \tag{12}$$

$$I_{X3} = m_3\left[\frac{1}{12}l_3^2 + \frac{1}{4}(r_2^2 + r_1^2) + (l_3/2 - \bar{z})^2\right] \tag{13}$$

From the parallel-axis theorem, the moment of inertia on the X axis for the rotating ring becomes:

$$I_X = I_{X1} + I_{X2} + I_{X3} \tag{14}$$

33) Saw Toothed Supported Type

34) Both End Trapezoidal Type

35) Both End Triangular Type

36) Both End Inverse Triangular Type

37) Zigzag Type 1

38) Zigzag Type 2

39) Both End Saw Toothed Type

40) Top Type

41) Mixed Type 1

42) Mixed Type 2

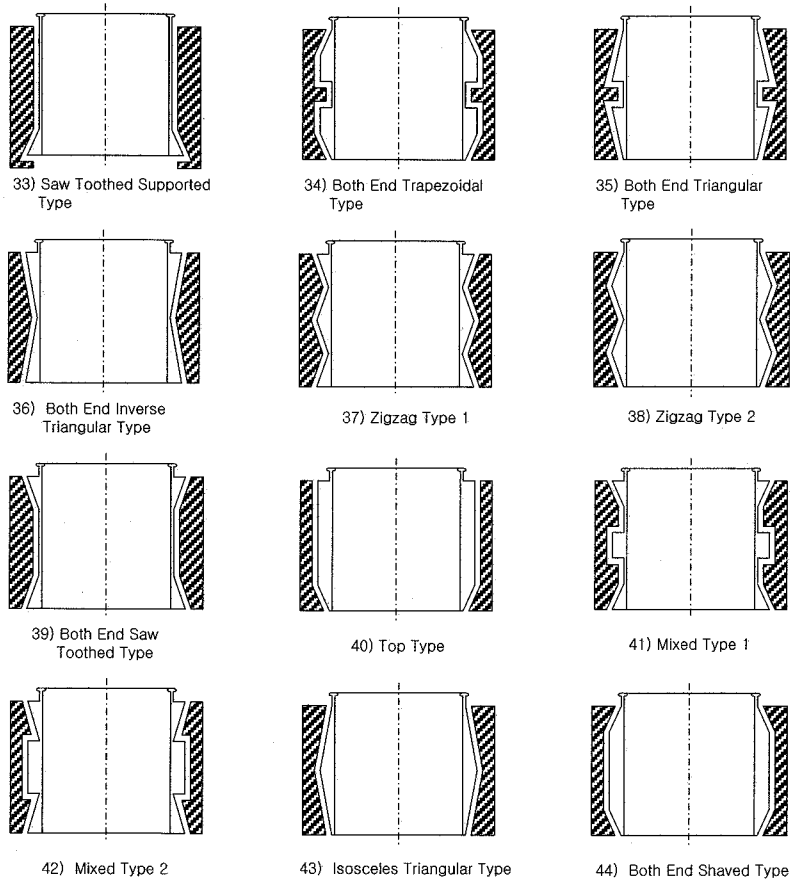43) Isosceles Triangular Type

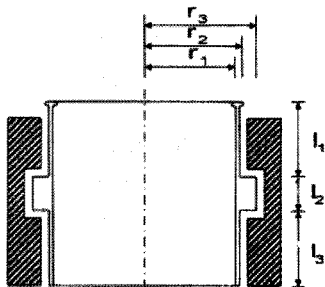44) Both End Shaved Type

Fig. 3 Rotating ring shape (3)

Fig. 4 Dimensions of a rotating ring of the one-stage rectangular (convex) type

The moment of inertia on the Z axis for each part of the rotating ring(d_1, d_2, d_3) can be obtained by the following equations, respectively:

$$I_{Z1} = \frac{1}{2}m_1(r_2^2 + r_1^2) \tag{15}$$

$$I_{Z2} = \frac{1}{2}m_2(r_3^2 + r_1^2) \tag{16}$$

$$I_{Z3} = \frac{1}{2}m_3(r_2^2 + r_1^2) \tag{17}$$

The moment of inertia ratio on the Z axis can be expressed as follows using the parallel-axis theorem:

$$I_z = I_{Z1} + I_{Z2} + I_{Z3} \tag{18}$$

MIR is defined by Equation (19):

$$MIR = \frac{I_X}{I_z} \tag{19}$$

The moment of inertia ratios from Fig. 3 (2) to Fig. 3 (44) are also derived using a method similar to that described above.

4. Computation of MIR values and detailed design of a rotating ring

The MIR values for forty-four rotating rings have been computed by MATLAB.

Table 1 gives the computed values of the MIR for the suggested rotating rings. From this table, it was found that there were no rotating rings which had a MIR value larger than 1.0. This means that the processional motion can not be removed completely from the ring motion in the yarn spinning process. The values of the MIR for a rotating ring of one-stage type are almost the same as those of the two-stage type. However, the values of MIR for a rotating ring of the concave type were larger than those of the convex type. Finally, as shown in this table, the rotating ring of a saw-toothed supporting(STS) type had the largest MIR value of 0.8408.

On the basis of the STS type rotating ring, a detailed design of rotating ring was conducted by changing the height and thickness of the rotating ring while considering the ordinary ring spinning system. The results of the detailed design are depicted in Fig. 5(MIR=0.8426). In this figure, r_1, r_2, r_3, and MIR are 22mm, 24mm, 26mm and 0.8426, respectively.

Table 1 Values of the Moment of inertia ratio (MIR)

| Rotating Ring Type	MIR	Rotating Ring Type	MIR
One-Stage Rectangular Type (convex)	0.7020	Two-Stage Rectangular Type (convex)	0.6577
One-Stage Rectangular Type (concave)	0.7930	Two-Stage Rectangular Type (concave)	0.7005
One-Stage Triangular Type (convex)	0.7456	Two-Stage Triangular Type (convex)	0.7386
One-Stage Triangular Type (concave)	0.7519	Two-Stage Triangular Type (concave)	0.7555
One-Stage Half Circular Type (convex)	0.5775	Two-Stage Half Circular Type (convex)	0.7147
One-Stage Half Circular Type (concave)	0.7851	Two-Stage Half Circular Type (concave)	0.7985
One-Stage Pentagonal Type (convex)	0.7232	Two-Stage Pentagonal Type (convex)	0.7186
One-Stage Pentagonal Type (concave)	0.7840	Two-Stage Pentagonal Type (concave)	0.7969
One-Stage Saw-Toothed Type (convex)	0.7463	Two-Stage Saw-Toothed Type (convex)	0.7397
One-Stage Saw-Toothed Type (concave)	0.7717	Two Stage Saw-Toothed Type (concave)	0.7725
One-Stage Trumpet Type (convex)	0.6810	Two-Stage Trumpet Type (convex)	0.6984
One-Stage Trumpet Type (concave)	0.7910	Two-Stage Trumpet Type (concave)	0.8065
One-Stage Trapezoidal Type (convex)	0.7236	Two-Stage Trapezoidal Type (convex)	0.6653
One-Stage Trapezoidal Type (concave)	0.7827	Two-Stage Trapezoidal Type (concave)	0.8218
One-Stage Equilateral Trapezoidal Type (convex)	0.7030	Two-Stage Equilateral Trapezoidal Type (convex)	0.5487
One-Stage Equilateral Trapezoidal Type (concave)	0.8006	Two-Stage Equilateral Trapezoidal Type (concave)	0.8300
Saw-Toothed Supporting Type	0.8408	Both End Saw-Toothed Type	0.8200
Both End Trapezoidal Type	0.7395	Top Type	0.7795
Both End Triangular Type	0.7395	Mixed Type 1	0.8017
Both End Inverse Triangular Type	0.8400	Mixed Type 2	0.7586
Zigzag Type 1	0.7919	Isosceles Triangular Type	0.7003
Zigzag Type 2	0.7552	Both End Shaved Type	0.7081
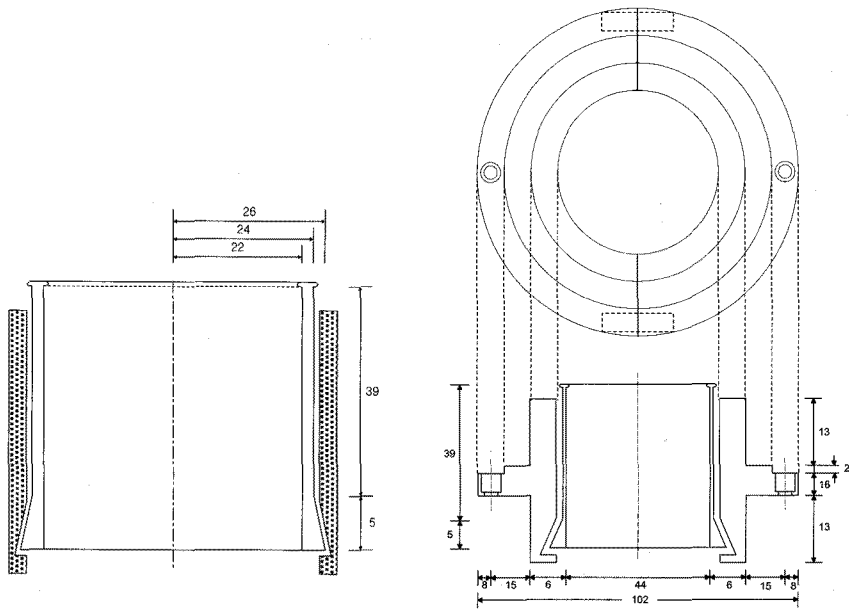
Fig. 5 Results of the optimal design for a rotating ring

5. Experiment

The STS type rotating ring which was manufactured for this research is shown in Photo 1. PET 340 Den./100 Fil.(320 T.P.M.) was used as the fiber material in the experiment. The measuring system used to measure the yarn tension and the vibration of the rotating ring in the yarn spinning process is shown in Fig. 1 and Fig. 6. Also, the specification of yarn tension sensor is shown in Table 2.

In this figure, the sensor head (1) measured the vertical vibration of the rotating ring and the sensor head (2) measured the horizontal vibration of the rotating ring. A tiny projection was set on the rotating ring to measure the rotational speed of the rotating ring. By this projection, the signal peak will have appeared either in the vertical or horizontal vibration signals for every rotation. The rotational speed of the rotating ring was obtained based on the time interval of these peaks. Fig. 7 shows the horizontal signal of the rotating ring in the spinning process(spindle speed is 150000rpm).

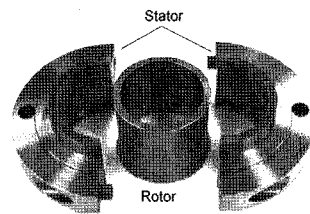The sensor that detected the spinning tension was set
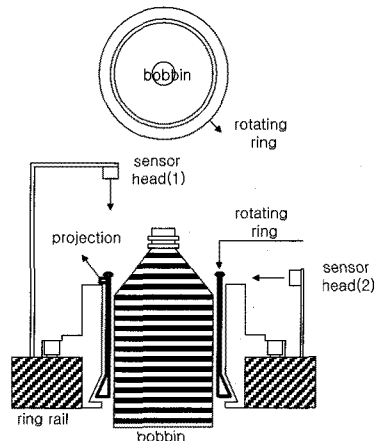

Photo. 1 Developed rotating ring

Fig. 6 Schematic diagram of the experimental apparatus

Table 2 Specification of yarn tension sensor

Load cell input voltage	DC 5V
Input intensity	0.3 μV/D
Non-linearity	0.01% F.S. max
Input signal range	0mV~20 mV
Temperature coefficient	± 0.2 μV/℃ RTI Max
Input noise	± 0.3 μVpp
Input impedance	10MΩ
A/D Converter	Sigma delta type
A/D inner dissolution	1/200,000
A/D outer dissolution	1/10,000
Display	7-Segment(LCD), 4 1/2-Digits(17.8mm)
Display converting speed	10 times/sec
Power source	6AAA 1.2Volt ACCU
Power consumption	5VA
Data memory	10 years
Temperature range	-10℃~40℃

(a) Fixed ring

(b) Rotary ring

Fig. 8 Spinning tension of a conventional fixed ring and a rotating ring
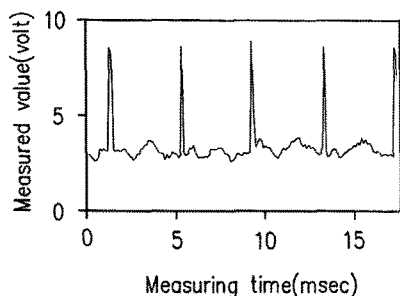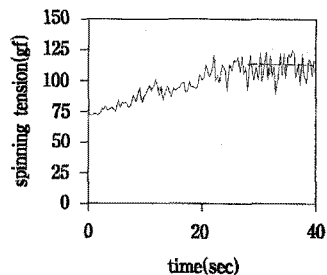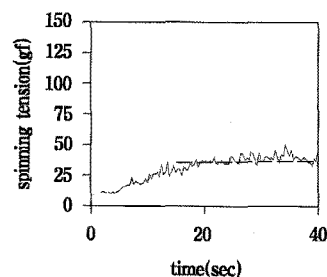

Fig. 7 Horizontal vibration of the rotating ring

at a position between the front roller and the snail wire (Fig. 1). The spinning tension of a conventional fixed ring and the newly developed STS type rotating ring are compared in Fig. 8. The average spinning tensions by the conventional fixed ring and STS type rotating ring were 113.7 g_f and 36.5 g_f, respectively. This experiment verified that a reduction in the spinning tension of up to 67.8% can be achieved using the STS type rotating ring.

6. Conclusions

In this paper the saw-toothed supporting(STS) type rotating ring has been designed and manufactured, which has dynamic stability in the ring spinning process. By applying this rotating ring to the conventional spinning system, the following results have been obtained.

(1) Forty-four kinds of rotating ring shapes which can be used in the ring spinning system have been proposed.

(2) The MIR values for the proposed 44 kinds of rotating ring shapes have been computed. By analyzing the computational results, it was found that the values of MIR for a rotating ring of the one-stage type are almost same as those of the two-stage type. The values of MIR for rotating rings of the concave type, however, are larger than those of the convex type.

(3) The saw-toothed supporting (STS) type rotating ring has the largest value of MIR of 0.8408 among the

proposed 44 kinds of rotating rings.

(4) On the basis of the STS type rotating ring, the shape of the rotating ring has been optimized considering the ordinary ring spinning system.

(5) Through experimentation, it was verified that the spinning tension could be reduced by 67.8% when using the newly developed rotating ring.

Nomenclature

a, b : coefficient of eccentric restoration force

l : height of rotating ring

f : spinning tension

g : gravity

G : center of rotational coordinate system

I_X, I_Y, I_Z : moment of inertia on X, Y and Z axes

MIR : moment of inertia ratio

m_r : mass of rotating ring

m_t : mass of traveller

O : center of fixed coordinate system

r_0 : rotational speed of rotating ring

r_t : rotational speed of traveller

r_1 : inner radius of rotating ring

r_2 : outer radius of rotating ring

r_3 : distance from the center of the rotating ring to the edge

t : time

X, Y, Z : fixed coordinate system

X', Y', Z' : rotational coordinate system

$\bar{z}$: position of center of gravity

α, β, γ : rotational angle of rotating ring around the X, Y and Z axes

η : coefficient of air resistance

μ : frictional coefficient between rotating ring and traveller

θ : rotational angle of traveller around Z axis ($=r_t \cdot t$)

τ_s : torque by friction between rotating ring and stator

ρ : density of rotating ring

References

(1) Igel, W., 1979, "Luftgelagerte Spinnringe," Textil Praxis International(in German), Vol. 34, pp. 1093~1096.

(2) McPhee, J. R., Russell, K. P., and Shaw, T., 1985, "The role of objective measurement in the wool-textile industry," *the Journal of the Textile Institute*, Vol. 76, No. 2, pp. 110~121.

(3) Jang, S. H. and Huh, Y., 1995, "Modeling of rotating ring dynamics with point pulsating force," *Journal of the Korean Fiber Society*, Vol. 32, No. 9, pp. 853~857.

(4) Jang, S. H., Kwon, Y. H., and Huh, Y., 1995, "Experimental analysis on the vibration of rotating ring," *Journal of the Korean Fiber Society*, Vol. 32, No. 10, pp. 934~940.

(5) Jang, S. H. and Nakajima, N., 1992, "Study of the CAE system for product development," *JSME International Journal*, Vol. 35, No. 3, pp. 493~499.

(6) Jang, S. H., 1996, "Vibrational characteristics of annular plates and rings of radially varying thickness," *KSME Journal*, Vol. 10, No. 2, pp. 146~157.

(7) Jang, S. H., 2008, "S. H. Jang, A Study on three dimensional layout design by the simulated annealing method," *Journal of Mechanical Science and Technology*, Vol. 22, pp. 2016~2023.

(8) Lee, Y., Jeong, J., Kim, H., and Shin, K., 2009, "An experimental study on the failure characteristics of flip chips in cyclic bending test," *Journal of the Korean Society of Machine Tool Engineers*, Vol. 18, No. 4, pp. 362~368.

(9) Cho, B. and Seong H, 2010, "The Design of sliding mode controller for precision stage using genetic algorithm," *Journal of the Korean Society of Machine Tool Engineers*, Vol. 19, No.1, pp. 101~109.

(10) Song, J., Mun, S., Kim, Y., and Kim, H., 2010, "Compressive strength of natural fiber reinforced polymer composites," *Journal of the Korean Society of Machine Tool Engineers*, Vol. 19, No. 1, pp. 140~144.